RSC Advances

PAPER

View Article Online
View Journal | View Issue

Check for updates

Cite this: *RSC Adv.*, 2018, **8**, 21671

A novel microporous Tb-MOF fluorescent sensor for highly selective and sensitive detection of picric acid†

Ping Ju, ‡[a] Ensheng Zhang, ‡*[a] Long Jiang,[b] Ze Zhang,[a] Xiangyang Hou,[a] Yuqi Zhang,[a] Hua Yang[a] and Jijiang Wang *[a]

Received 26th March 2018
Accepted 24th May 2018

DOI: 10.1039/c8ra02602e

rsc.li/rsc-advances

A new three-dimensional metal–organic framework (MOF) sensor with molecular formula $(C_2H_6NH_2)_2[Tb_2(ptptc)_2(DMF)(H_2O)]\cdot DMF\cdot 6H_2O$ (complex **1**) has been constructed from terphenyl-3,3′,5,5′-tetracarboxylic acid (H_4ptptc) and terbium nitrate under solvothermal conditions. The structure of complex **1** was characterized by single-crystal X-ray diffraction analysis (XRD), elemental analysis, IR spectroscopy and thermogravimetric (TG) analysis, and the purity was further confirmed by powder X-ray diffraction (PXRD) analysis. XRD analysis reveals that complex **1** crystallizes in a triclinic system $P\bar{1}$ space group and consists of a three-dimensional anionic network which has one-dimensional channels. Fluorescence titration experiments showed that complex **1** displayed real-time, highly selective and sensitive fluorescence quenching behavior towards picric acid with a nanomolar scale experimental detection limit (100 nM). Recycling titration experiments suggested that the as-synthesized probe has good reversibility and can be used for at least five cycles in fluorescence titration experiments without obvious fluorescence intensity reduction or framework structure destruction. Furthermore, the high selectivity and sensitivity as well as good recyclability of complex **1** make it a potential fluorescent sensor for picric acid.

Open Access Article. Published on 13 June 2018. Downloaded on 5/2/2026 9:02:42 AM.
This article is licensed under a Creative Commons Attribution-NonCommercial 3.0 Unported Licence.

1 Introduction

Picric acid (PA) is one of the most well-known explosives with high explosive detonation properties and a low safety coefficient. As an important crude substance, PA has been widely used in the manufacture of commodities such as rocket fuels,[1] fireworks,[2] matches,[3] dyes,[4] medicines and pesticides.[5] However, due to its strong explosive capacity, PA could also be used for military applications and terrorist attacks. The heavy use of PA has caused severe problems such as catastrophic environmental pollution,[6] public health issues[7] and homeland security problems. Hence, rapid detection of PA is attracting increasing attention.[8]

In the past few decades, various sophisticated methods such as high performance liquid chromatography (HPLC),[9] Raman spectroscopy[10] and ion-mobility spectroscopy (IMS),[11] *etc.* have been established for the detection of nitrogen containing aromatic explosives including picric acid. Although significant progresses have been made for the above mentioned analytical techniques some drawbacks such as high cost, less selectivity and not real-time monitoring limit their practical applications. Luckily, fluorescence sensors have emerged as promising analytic tools for the detection of picric acid in the past few years, for example, various functional small organic molecules,[12] metal or nonmetal nanoparticles,[13] luminescent quantum dots[14] were designed for PA detection. It is worth mention that luminescent metal–organic frameworks (MOFs) have emerged as promising chemosensors for PA detection in the past few years, and the design, synthesis and application study of luminescent MOFs sensors has drawn great attentions.[15] Despite significant progresses have been made in the development of fluorescent luminescent MOFs sensor for picric acid there is still scope for improvement, especially, the recyclable real-time fluorescence sensors with high selectivity and sensitivity are still high desirable.

In this work, we report a new three-dimensional (3D) metal–organic framework sensor with the molecular formula $(C_2H_6NH_2)_2[Tb_2(ptptc)_2(DMF)(H_2O)]\cdot DMF\cdot 6H_2O$ (complex **1**) for highly selective and sensitive detection of PA. Complex **1** was constructed with terphenyl-3,3′,5,5′-tetracarboxylic acid (H_4ptptc) and terbium nitrate under solvothermal conditions and characterized by XRD, elemental analysis, IR spectra, TG analysis. This 3D framework containing one-dimensional (1D) channels along *a* and *b* axis, which are expected to facile the diffusion and concentration of analytes and the host–guest interactions. Instant fluorescent responds were detected when complex **1** was

[a]*Laboratory of New Energy & New Function Materials, Shaanxi Key Laboratory of Chemical Reaction Engineering, College of Chemistry and Chemical Engineering, Yan'an University, Yan'an, Shaanxi, 716000, P. R. China. E-mail: sdzes2006@163.com; yadxwjj@126.com*

[b]*MOE Key Laboratory of Bioinorganic and Synthetic Chemistry, School of Chemistry and Chemical Engineering, Sun Yat-Sen University, Guangzhou 510275, P. R. China*

† Electronic supplementary information (ESI) available. CCDC 1828358. For ESI and crystallographic data in CIF or other electronic format see DOI: 10.1039/c8ra02602e

‡ Ping Ju and Ensheng Zhang equally contributed to this work.

Open Access Article. Published on 13 June 2018. Downloaded on 5/2/2026 9:02:42 AM. This article is licensed under a Creative Commons Attribution-NonCommercial 3.0 Unported Licence.

treated with PA and a nanomolar scale experimental detection limit (100 nM) was observed in the fluorescent titration experiments. According to the PXRD and fluorescent analysis for complex **1** after five cycles in fluorescence titration experiments, no obvious fluorescent intensity reducing or framework structure destruction was observed, which suggested the good recyclability of complex **1**. Noticeable features of this probe include: (1) recyclable and real-time sensor for PA detection; (2) high sensitivity and selectivity for PA detection; (3) potential fluorescent sensor for detection PA in water or solid state.

2 Experimental

2.1 Reagents and instruments

The ligand (H_4ptptc) and all the reagents were commercially available and used without further purification. Elemental analyses for C, H and N were carried out with a Vario EL elemental analyzer. The IR spectra were recorded on a Shimadzu IR Affinity-1S FTIR Spectrophotometer using the KBr pellet. The thermogravimetric analyses (TGA) were performed on a Netzsch TG-209 Thermogravimetry Analyzer in N_2 atmosphere. The Powder X-ray diffraction (PXRD) patterns were measured with a Bruker D8 ADVANCE X-Ray Diffractometer. Photoluminescence spectra were performed on an Agilent Cary Eclipse fluorescence spectrophotometer at room temperature. The luminescent lifetime study of the compound was carried out on an Edinburgh fluorescence spectrophotometer (Edinburgh Instruments FLS920)

2.2 Structure determination

The single-crystal data of **1** was collected on Bruker D8 Venture system, with Mo Kα radiation (λ = 0.71073 Å) at 150 K. All empirical absorption corrections were applied using the SCALE3 ABSPACK program.[16] The structure was solved by direct methods and refined by full-matrix least-squares analysis on F2 using the SHELX97 program package. All non-hydrogen atoms were refined anisotropically. The electron density of $Me_2NH_2^+$, DMF and H_2O molecules in **1** were treated as a diffuse contribution using the program SQUEEZE.[17] The hydrogen atoms were relocated in geometrically sensible positions after each refinement cycle and given thermal parameters defined by those applying to the atom to which they are attached. The C57 atom of lattice DMF molecule exhibits orientational disorder over two sets of positions (C57 and C57′) which lead to the low distance between H46A and H57A. All calculations were performed using the SHELXTL system of computer programs.[18] Crystallographic data and structure refinements for complex **1** were displayed in Table 1. The selected bond lengths and bond angles were summarized in Table 1S.† CCDC reference number of crystal **1** is 1828358.

2.3 Synthesis of $(C_2H_6NH_2)_2[Tb_2(ptptc)_2(DMF)(H_2O)]\cdot DMF\cdot 6H_2O$ (1)

$Tb(NO_3)_3\cdot 6H_2O$ (8.7 mg, 0.02 mmol), H_4ptptc (4 mg, 0.01 mmol) and HNO_3 (6 M, 3 d) were added to a 25 mL Teflon-lined stainless steel vessel. A 1 : 1 (v/v) mixture of DMF (4 mL) and H_2O (4 mL) was added to the mixture. The content was heated at 160 °C for 72 h. The colorless block-like crystals were obtained and washed with DMF, then dried in air (63% yield based on Tb). Anal. calcd for $C_{54}H_{64}N_4O_{25}Tb_2$ (%): C, 43.64; H, 4.31; N, 3.77. Found (%): C, 43.21; H, 4.02; N, 3.98.

Table 1 Crystal data and structure refinements for complex **1**

Compound reference	**1**
Formula	$C_{54}H_{64}N_4O_{25}Tb_2$
Fw	1486.93
Crystal system	Triclinic
Space group	$P\bar{1}$
a (Å)	10.8814(6)
b (Å)	16.0497(11)
c (Å)	19.4459(13)
α (°)	74.097(4)
β (°)	74.566(3)
γ (°)	72.105(3)
V (Å^3)	3046.1(3)
Z	2
D_c (g cm^{-3})	1.621
Reflections/Unique	11 171/7610
R(int)	0.1151
GOF on F^2	1.046
$^aR_1[I \geq 2\sigma(I)]$	0.0655
$^bwR_2[I \geq 2\sigma(I)]$	0.1597

^{a} $R_1 = \Sigma||F_o| - |F_c||/\Sigma|F_o|$. ^{b} $wR_2 = [\Sigma[w(F_o^2 - F_c^2)^2]/\Sigma w(F_o^2)^2]^{1/2}$, where $w = 1/[\sigma^2(F_o)^2 + (aP)^2 + bP]$ and $P = (F_o^2 + 2F_c^2)/3$.

2.4 Luminescence sensing experiments

2.4.1 Solvent selection. 2 mg powder sample of complex **1** was dispersed into 2 mL methanol (MeOH), ethanol (EtOH), acetone, acetonitrile (CH_3CN), *p*-xylene (PX), toluene, benzene, tetrahydrofuran (THF), chloroform ($CHCl_3$), dimethyl sulfoxide (DMSO), diethyl ether (Et_2O), petroleum ether (PE), dimethyl formamide (DMF), respectively. Suspensions were treated with ultrasonication prior to fluorescence measurements (λ_{ex} = 325 nm, slits: 5 nm/10 nm).

2.4.2 Selectivity study for PA. The stock solutions of *p*-nitrobenzoic acid (PNBA), *m*-nitroaniline (*m*-NA), *o*-nitroaniline (*o*-NA), *o*-nitrophenol (*o*-NP), picric acid (PA), nitrobenzene (NB), 2,4-dinitrophenylhydrazine (2,4-DNPH), benzene, phenol, aniline, 3-nicotinic acid (3-NC) were prepared in anhydrous methanol with the concentration of 10 mM. 2 mg powder sample of complex **1** was dispersed into methanol (2 mL) with ultrasonication to afford the suspension. The selectivity of this sensor was studied by treatment of the above suspensions with 50 μM different nitro compounds (PNBA, *m*-NA, *o*-NA, *o*-NP, PA, NB, 2,4-DNPH) or aromatic compounds (benzene, phenol, aniline, 3-NC) and recording the fluorescent intensity changes (λ_{ex} = 325 nm, slits: 5 nm/10 nm). In order to investigate the interference, the above suspensions were treated with 50 μM PA in the presence of 50 μM other analyses. The sensitivity was investigated by mixing the suspensions with 0–200 μM PA and recording the fluorescence intensity changes (λ_{ex} = 325 nm, slits: 5 nm/10 nm).

3 Results and discussion

3.1 Crystal structure description of complex 1

Single-crystal X-ray diffraction analysis reveals that complex **1** crystallizes in a triclinic system $P\bar{1}$ space group. As shown in

 This journal is © The Royal Society of Chemistry 2018

Open Access Article. Published on 13 June 2018. Downloaded on 5/2/2026 9:02:42 AM.
This article is licensed under a Creative Commons Attribution-NonCommercial 3.0 Unported Licence.

Fig. 1a, each asymmetric unit of **1** contains two Tb^{3+} ions, two $ptptc^{4-}$ ligands, one coordinated DMF, one coordinated water molecule, two dimethylammonium ions, one lattice DMF molecule and six lattice water molecules. Tb1 is nine-coordinated by six chelating carboxylate oxygen atoms, two bridging carboxylate oxygen atoms and one DMF molecule forming a distorted triangular tetrakaidecahedron geometry, Tb2 presents similar coordination environment to Tb1, while the difference is that it is coordinated by one H_2O molecule instead of DMF. The crystallographically independent nine-coordinated Tb1 and Tb2 are connected by a pair of carboxylate bridges to form $[Tb_2(\mu_2\text{-}COO)_2(COO)_6]^{2-}$ dimetallic units, with Tb···Tb distance being 5.521 Å (Fig. 1b). The Tb–O bond length is range from 2.268(7) Å to 2.578(7) Å, which are consistent with the reported complexes.[19] Individual dimetallic clusters are further connected by $ptptc^{4-}$ ligands to construct a three-dimensional (3D) anionic framework. The anionic framework is balanced by dimethylammonium counterions which were formed *in situ* in the reaction.[20]

In the crystal structure, $ptptc^{4-}$ ligands have two different coordination modes: the μ_6-coordination style which has two bridging bidentate and two chelating bidentate carboxylate groups and the μ_4-coordination style which has four chelating bidentate carboxylate groups. As shown in Fig. 2a, each $[Tb_2(\mu_2\text{-}COO)_2(COO)_6]^{2-}$ dimetallic unit connected with four μ_6-coordination $ptptc^{4-}$ ligands forming a 2D layer structure on *ab* plane. The μ_4-coordination $ptptc^{4-}$ ligands connect the parallel layers upward and downward to form a 3D porous structure with one-dimensional (1D) channels. This 3D framework contains 1D tetragonal channels along *a* axis with the sizes of 8.0 Å × 8.0 Å (Fig. 2b) and two kind of 1D channels in *b* axis with the sizes of 8.3 Å × 10.0 Å (rectangular channel) and 9.0 Å × 11.0 Å (rhomboid channel), respectively (Fig. 2c). Counterionic dimethylammonium, coordinated molecules and lattice solvent molecules are filled in these channels, and 35% solvent-accessible volume was estimated by using the PLATON program.[21]

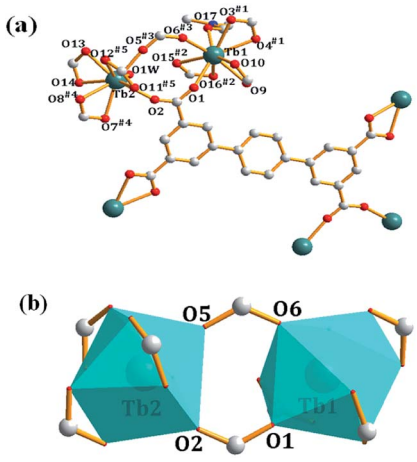

Fig. 1 (a) Coordination environments of Tb1 and Tb2 in complex **1**, guests and hydrogen atoms are omitted for clarity; (b) the coordination polyhedron of $[Tb_2(\mu_2\text{-}COO)_2(COO)_6]^{2-}$. (Symmetry codes: (#1) $-1+x, y, z$; (#2) $-x, -y, -z+1$; (#3) $x, -1+y, z$; (#4) $x+1, -1+y, z$; (#5) $1-x, -y, 2-z$; (#6) $1+x, y, z$; (#7) $-1+x, 1+y, z$; (#8) $1-x, 1-y, 2-z$; (#9) $2-x, -1-y, 1-z$; (#10) $x, 1+y, z$).

3.2 PXRD, IR and TG analyses

3.2.1 PXRD analyses. The purity of the bulky crystalline samples of complex **1** was confirmed by PXRD at room temperature. As shown in Fig. 8b, the PXRD pattern of as-synthesized complex **1** match well with the simulated one based on the single-crystal diffraction data, which confirming the good purity of complex **1**.

3.2.2 IR spectra. IR spectra of the compound **1** and H_4ptptc were obtained and displayed in Fig. 1S.† The broad absorption centered at 3420 cm^{-1} could attribute to the O–H stretching vibrations of the water molecules. As expected, compared with H_4ptptc a red shift (about 40 cm^{-1}) were observed for the characteristic stretching vibrations of carboxylate groups in complex **1**, which are coordinated with Tb1 and Tb2. As shown in Fig. 1S,† the peaks at 1657 cm^{-1} and 1630 cm^{-1} are assigned to the characteristic asymmetric stretching vibrations of the coordinate carboxylate groups Fig. 1S(a).† While the characteristic band around 1700 cm^{-1} could be attributed to the asymmetric stretching vibrations of carboxylate groups in H_4ptptc Fig. 1S(b).†

3.2.3 TG analysis. To evaluate the stability of **1**, the thermogravimetric analysis (TGA) was performed. The first weight loss of 6.27% was observed from room temperature to 100 °C in the TGA curve (ESI, Fig. 2S†), which corresponds to the release of

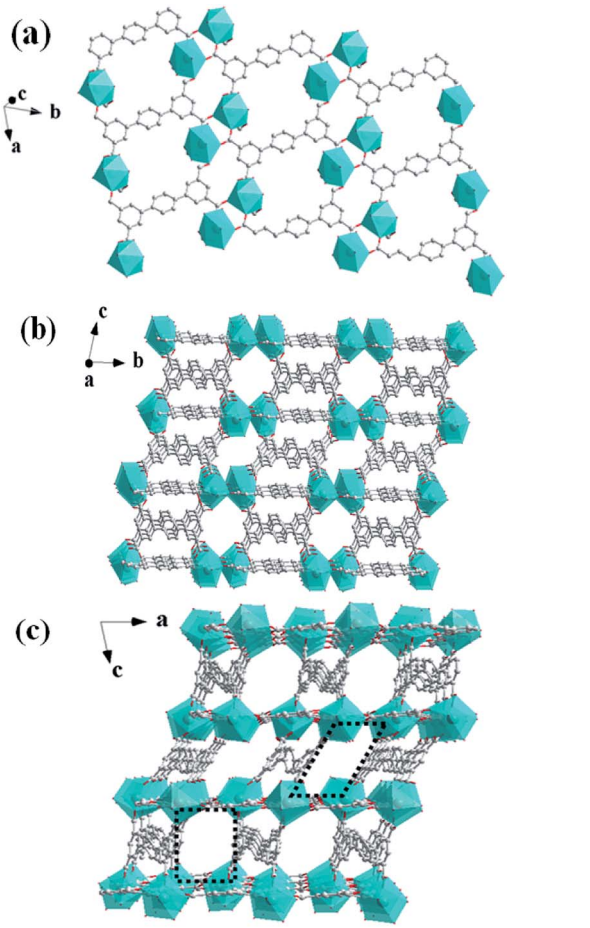

Fig. 2 (a) The 2D layer structure of **1** along the *ab* plane. (b) The 3D framework of **1** along the *bc* plane. (c) The 3D framework of **1** with 1D channels along the *ac* plane.

Open Access Article. Published on 13 June 2018. Downloaded on 5/2/2026 9:02:42 AM.
This article is licensed under a Creative Commons Attribution-NonCommercial 3.0 Unported Licence.

non-coordinated water molecules (calcd 7.26%) in the channels. The discrepancy between the found and theoretical values could be attributed to the loss of the lattice water at room temperature. The second weight loss is 11.17% at 100 ~ 199 °C, corresponding to the release of non-coordinated DMF molecules, coordinated H_2O and DMF molecules (calcd 11.03%); upon further heating, the desolvated framework is stable up to 375 °C, then the remaining framework start to collapse after that temperature.

3.3 Solid-state photoluminescent spectra

The solid-state fluorescence spectra of complex **1** and H_4ptptc were recorded on an Agilent Cary Eclipse fluorescence spectrophotometer with excitation at 325 nm at room temperature (slits: 5 nm/10 nm). As depicted in Fig. 3, the ligand displays a broad band emission range from 350 nm to 500 nm, which centered at about 419 nm. This emission could be assigned to the intra-ligand π–π* transitions.[22] Compound **1** exhibits a similar broad band emission with a lager blue-shift compared with H_4ptptc and maximum at 363 nm (λ_{ex} = 325 nm), which may be attributed to the complexation effect between H_4ptptc and Tb^{3+}. It is worth mentioning that the emission spectra of compound exhibits typical Tb red emissions and four well-resolved peaks were observed, which are centered at 491 nm, 546 nm, 586 nm and 621 nm, respectively. The characteristic emissions could be attributed to the corresponding transitions from $^5D_4 \rightarrow {}^7F_6$, $^5D_4 \rightarrow {}^7F_5$, $^5D_4 \rightarrow {}^7F_4$ and $^5D_4 \rightarrow {}^7F_3$ of Tb.[23]

3.4 Fluorescence sensing properties of complex 1

3.4.1 Solvent selection. In order to obtain a suitable solvent system for sensing property studies, the fluorescence property of complex **1** in different solvents (MeOH, EtOH, acetone, CH_3CN, PX, toluene, benzene, THF, $CHCl_3$, DMSO, Et_2O, PE, DMF; λ_{ex} = 325 nm, slits: 5 nm/10 nm) was studied. As shown in Fig. 4, the fluorescence intensity changed when the dispersing solvents were changed, but the positions of the maximum emission have no obvious change. It is obviously that the suspension of complex **1** showed the strongest emission in methanol and the weakest in acetone. Hence, methanol was chose as the optimized solvent for all the fluorescent titration experiments. It is worth mention that all the five emission bands were remarkably quenched when complex **1** was dispersed in acetone as depicted in Fig. 4, which revealed that complex **1** might be used as an indicator for acetone. In addition, both the solid-state fluorescence property and the luminescence of complex **1** in solvents promote us to investigate its potential application in the detection of small organic molecules.

3.4.2 Selectivity of complex 1 for aromatic in methanol. The luminescent responses of complex **1** were investigated by treating 1-methanol suspensions (2 mg dispersed in 2 mL methanol) with 50 μM different analytes such as *p*-nitrobenzoic acid (PNBA), *m*-nitroaniline (*m*-NA), *o*-nitroaniline (*o*-NA), *o*-nitrophenol (*o*-NP), picric acid (PA), nitrobenzene (NB), 2,4-dinitrophenylhydrazine (2,4-DNPH), benzene, phenol, aniline and 3-nicotinic acid (3-NC), respectively. The fluorescent responses (F_0/F or I_0/I) centered at 363 nm, 491 nm, 546 nm, 586 nm and 621 nm of complex **1** in methanol after addition of different aromatics were displayed in Fig. 5a (F_0/F, F_0 is the fluorescent intensity of the suspension without analytes and F is the fluorescent intensity of the suspension in the presence of analytes). It is obviously form Fig. 5a, the five emission bands of complex **1** exhibited remarkable fluorescent quench phenomenon only when adding PA to the suspension, which clearly suggests the good selectivity of complex **1** toward PA. Interestingly, the relative fluorescent intensities of the emission bands are strongly dependent on the nature of the aromatics. For instance, no obvious quench effect was observed for PNBA and only slight quench effects were observed when adding *m*-NA, *o*-NA, *o*-NP, nitrobenzene (NB), 2,4-DNPH, benzene, phenol, aniline and 3-NC. Furthermore, the quench effect for the emission at 363 nm is much higher with respect to the characteristic emissions of Tb (centered at 491 nm, 546 nm, 586 nm and 621 nm), however, contrary phenomenon was observed for other aromatics. This could be attributed to the stronger electron transfer effect between $ptptc^{4-}$ and PA than that of other aromatics. Hence, the spectral intensity emitted by electron

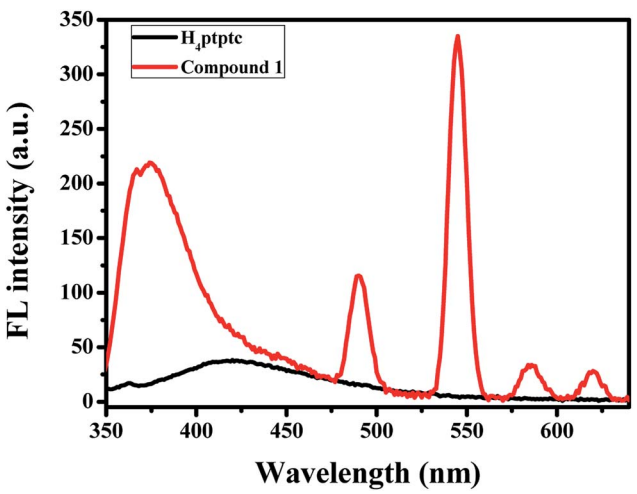

Fig. 3 Solid-state photoluminescent spectra of compound **1** and H_4ptptc at room temperature (λ_{ex} = 325 nm).

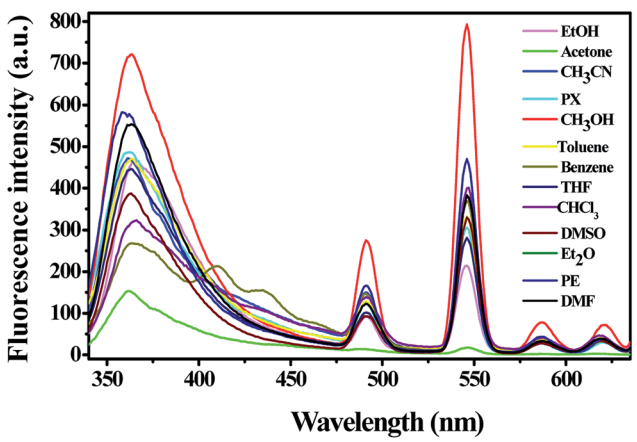

Fig. 4 Fluorescent intensity of 2 mg complex **1** dispersed in different solvents (λ_{ex} = 325 nm, slits: 5 nm/10 nm).

This journal is © The Royal Society of Chemistry 2018

Open Access Article. Published on 13 June 2018. Downloaded on 5/2/2026 9:02:42 AM.
This article is licensed under a Creative Commons Attribution-NonCommercial 3.0 Unported Licence.

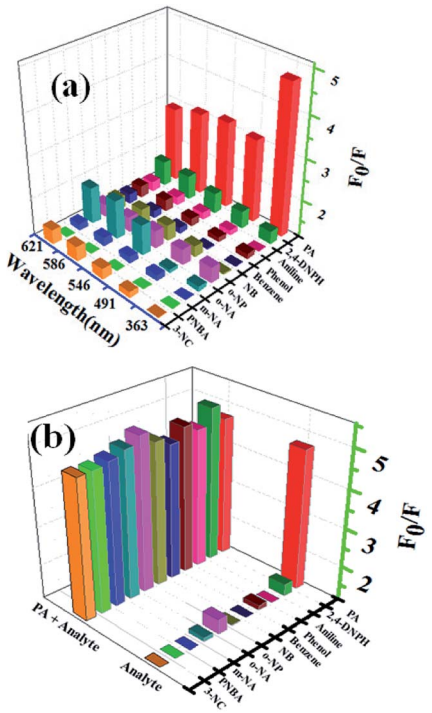

Fig. 5 (a) Fluorescent intensity of methanol suspensions of complex **1** with 50 μM different analytes (λ_{ex} = 325 nm, slits: 5 nm/10 nm); (b) fluorescent intensity of 1-methanol suspensions at 363 nm with 50 μM different analytes in the absence and presence of 50 μM PA.

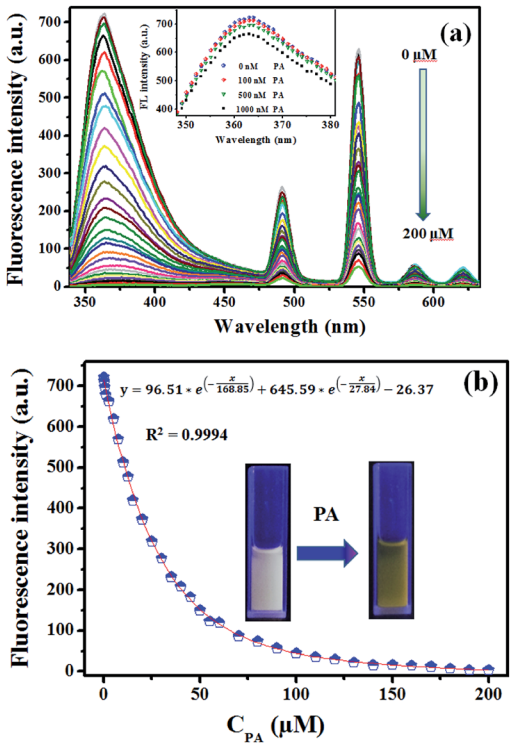

Fig. 6 (a) Fluorescence response of **1** towards different concentration of PA in methanol (λ_{ex} = 325 nm, λ_{em} = 363 nm, λ_{em} = 491 nm, λ_{em} = 546 nm, λ_{em} = 586 nm, λ_{em} = 621 nm, slits: 5 nm/10 nm); inset: fluorescence intensity of 1-methanol suspensions after treated with PA (0–1000 nM); (b) nonlinear fitting analysis of fluorescence intensity of 1-methanol suspensions *versus* the concentration of PA (λ_{ex} = 325 nm, λ_{em} = 363 nm, slits: 5 nm/10 nm); inset: photographs of 1-methanol suspensions in the absence and presence of PA under 254 nm luminescent lamp.

transition of ptptc^{4-} π–π* located at 363 nm was monitored for further investigate of the sensing ability of complex **1** for PA.

The fluorescent intensity of 1-methanol suspensions with 50 μM PA in the absence and presence of different aromatics (50 μM) were recorded and displayed in Fig. 5b (emission centered at 363 nm). It is obviously that no significant change of the fluorescence intensity for 1-methanol suspensions was observed in the presence of other analytes, which indicated that the selectivity of complex **1** toward PA over other competitive analytes is remarkably high.

3.4.3 Sensitivity investigation of complex 1. The sensitivity studies of complex **1** for PA were carried out by observing the fluorescence spectra of complex **1** in methanol with different concentration of PA (0–200 μM). And all the fluorescence spectra were recorded at 30 seconds after addition of PA at room temperature (1-methanol suspensions will take about 30 seconds to achieve steady fluorescence intensity after addition of PA according to Fig. 3S†).

The titration measurements were performed by incremental addition of 1 mM or 10 mM PA stock solutions into the methanol suspension of complex **1**. As shown in Fig. 6a, with increasing the concentration of PA (0.1–200 μM) the fluorescent intensity of 1-methanol suspensions steadily decreased (area enlarged view in Fig. 4S†). In order to further investigate the fluorescent titration effect of PA, the spectral intensity emitted by π–π* electron transition of ptptc^{4-} located at 363 nm was monitored. It is delight to notice that remarkable quench effect was observed and the quenching efficiency is about 99.45% which was calculated by using the equation $(1 - F/F_0) \times 100\%$ (F_0 is the initial fluorescence intensity of 1-methanol suspensions and F is the fluorescence intensity after addition of 200 μM PA).[24] It is worth mentioning that noticeable fluorescence quenching was already observed when 1-methanol suspension was treated with 100 nM PA, which revealed that the high sensitivity of complex **1** for PA (Fig. 6a, inset). Nonlinear fitting analysis for the fluorescence intensity of 1-methanol suspensions *versus* the concentration of PA (λ_{ex} = 325 nm, λ_{em} = 363 nm, slits: 5 nm/10 nm) was obtained and displayed in Fig. 6b. As depicted in Fig. 6b, the experimental data fitted well with the following non-linear equation:[25]

$$y = 96.51\, e^{\left(-\frac{x}{168.85}\right)} + 645.59\, e^{\left(-\frac{x}{27.84}\right)} - 26.37 \quad (R^2 = 0.9994),$$

revealing the potential application of complex **1** in quantitative analysis of PA.

High fluorescence quenching efficiency was also proved by the high Stern–Volmer binding constant (K_{sv} = 38 910), which was obtained by a steady-state fluorescence measurement.[26] As shown in Fig. 7 inset, good linearity of the plot at low concentrations of PA was observed which was fitted well with the Stern–Volmer equation: $I_0/I = 1 + K_{sv} \times [PA]$ (I_0 and I are the fluorescent intensities of 1-methanol suspensions in the absence and presence of PA, respectively; K_{sv} is the Stern–Volmer binding constant; [PA] is the molar concentration of PA).[27] The good linearity of Stern–Volmer

Open Access Article. Published on 13 June 2018. Downloaded on 5/2/2026 9:02:42 AM.
This article is licensed under a Creative Commons Attribution-NonCommercial 3.0 Unported Licence.

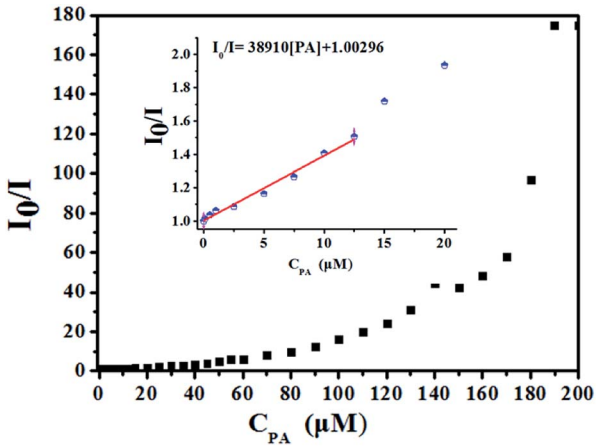

Fig. 7 Stern–Volmer plot of I_0/I *versus* the concentration of PA in 1-methanol suspension (inset: area enlarged view for linearity of the plot at lower concentrations of PA).

plot for PA at low concentrations indicating that there is only one type quenching process either dynamic or static quenching. However, as depicted in Fig. 7, a nonlinear curvature at higher concentrations of PA was obtained, revealing both the dynamic and static quenching is taking place.[28]

3.5 Recyclability study of complex 1

Recyclability is one of the most important parameter to assess the chemosensors practicability.[29] In order to reveal the recyclability of the as-synthesis potential sensor (complex **1**), the reproducibility study of the fluorescent detection activity was also carried out. Complex **1** was recovered by centrifugation followed by washing with methanol and used in the next cycle. It is shown in Fig. 8a, the fluorescence intensity of complex **1** does not decreased obviously after five cycles of continuously PA titration, which revealed that the as-synthesis MOF-sensor has good recyclability for PA detection. Furthermore, the purity of the recycled powder sample was determined by the powder X-ray diffraction and displayed in Fig. 8b. To our pleasant surprise, the PXRD test of complex **1** after five cycles (the top pattern in Fig. 8b) displayed a similar pattern as before and matched well with the simulated PXRD pattern which was obtained from the single-crystal X-ray diffraction data, but the intensity of peaks are decreased to some extent. All the above tests revealed that complex **1** has good potential for the practical use as a chemosensor for PA detection in terms of recyclability and stability.

3.6 Practical applications

3.6.1 Complex 1 coated test strips for the detection of PA in water. In order to reveal the potential application of this sensor, complex **1** coated test strips were prepared and used for the detection of PA in water.[30] Fig. 9 (a, left) shows the complex **1** coated test strips under sunlight and Fig. 9 (a, middle) displayed the same papers under 254 nm UV light in the absence of PA. It is obviously that bright fluorescence was observed for the test papers in the absence of PA. As shown in Fig. 9 (a, right), the

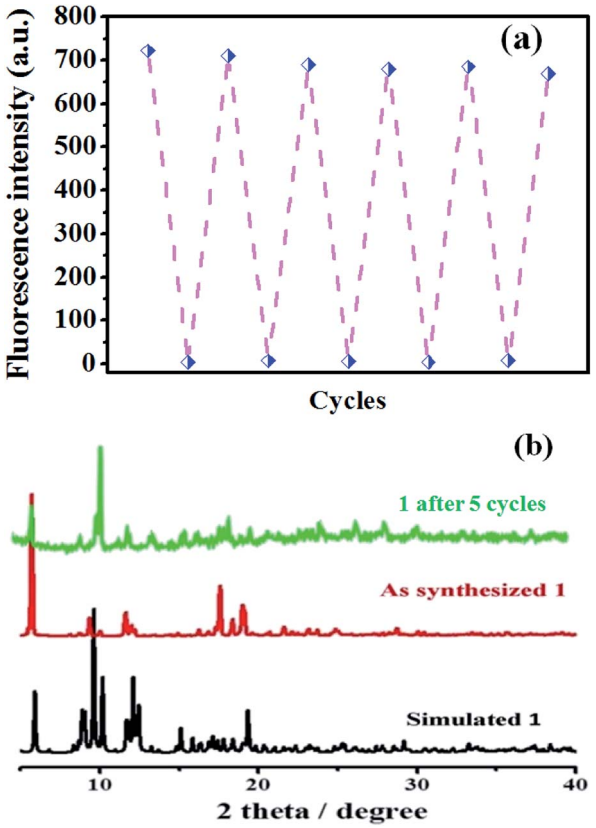

Fig. 8 (a) Reusability study of compound **1** for the detection of PA; (b) PXRD patterns of compound **1** before and after PA detection for 5 cycles, compared with the simulated pattern.

bright fluorescence of text papers remarkably quenched after immersed into PA solutions (5 μM, 50 μM, 500 μM, 5000 μM) for 30 seconds. It is noteworthy that the differentiable concentrations of PA for naked eyes under portable UV light (254 nm) based on fluorescent intensity changes can be as low as 5.0×10^{-6} M.

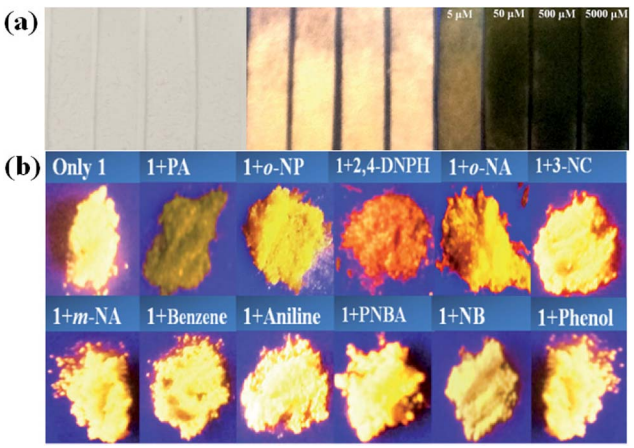

Fig. 9 (a) Complex **1** coated test strips under sunlight (left) and 254 nm UV light in the absence of PA (middle) and presence of PA (right); (b) photographs of complex **1** powdered samples under 254 nm UV light before and after mixture with different analytes.

This journal is © The Royal Society of Chemistry 2018

Open Access Article. Published on 13 June 2018. Downloaded on 5/2/2026 9:02:42 AM.
This article is licensed under a Creative Commons Attribution-NonCommercial 3.0 Unported Licence.

3.6.2 Solid state fluorescence quenching experiments. The potential application of this sensor was further studied by recording the fluorescent response of different analytes towards powdered microcrystalline of complex **1**. Fig. 9b shows the photographs of complex **1** powder samples in the absence or presence of different analytes under 254 nm UV light. It is apparently that obvious change was seen only for PA with the bright emission quenched completely.

4 Conclusion

A new strong fluorescent 3D metal–organic framework sensor (complex **1**) was successfully designed and synthesized using a highly π-conjugated organic ligand (H_4ptptc) and terbium nitrate under solvothermal conditions. The high selectively of complex **1** for PA was proved by steady-state fluorescence titration experiments and the experimental detection limit was found to be 100 nM, which indicating high detection sensitivity. Moreover, high quenching constant ($K_{sv} = 38\,910$) and excellent fluorescence quenching efficiency (99.45%) for PA were also observed in the fluorescence titration experiments. The recyclability experiments combine with PXRD tests reveal the good reusability of complex **1** for infield and real-time detection of PA. In addition, practical applications of complex **1** were confirmed by test strips and solid state fluorescence quenching experiments which imply complex **1** was a promising sensor for the practical detection of PA.

Conflicts of interest

There are no conflicts to declare.

Acknowledgements

This work was supported by Natural Science Foundation of China (21663032), Scientific Research Program Funded by Shaanxi Provincial Education Department (Program No. 17JK0869), Startup Foundation for Doctors and Youth Science Foundation of Yan'an University (YDBK2015-06, YDBY2016-001, YDQ2017-14).

References

1 J. Shen, J. Zhang, Y. Zuo, L. Wang, X. Sun, J. Li, W. Han and R. He, *J. Hazard. Mater.*, 2009, **163**, 1199–1206.
2 V. Bhalla, A. Gupta, M. Kumar, D. S. Rao and S. K. Prasad, *ACS Appl. Mater. Interfaces*, 2013, **5**(3), 672–679.
3 V. Bhalla, S. Kaur, V. Vij and M. Kumar, *Inorg. Chem.*, 2013, **52**(9), 4860–4865.
4 E. H. Volwiler, *Ind. Eng. Chem.*, 1926, **18**(12), 1336–1337.
5 P. G. Thorne and T. F. Jenkins, *Field Anal. Chem. Technol.*, 1997, **1**(3), 165–170.
6 Y. J. Hu, S. Z. Tan, G. L. Shen and R. Q. Yu, *Anal. Chim. Acta*, 2006, **570**(2), 170–175.
7 B. Roy, A. K. Bar, B. Gole and P. S. Mukherjee, *J. Org. Chem.*, 2013, **78**(3), 1306–1310.
8 (*a*) B. Joarder, A. V. Desai, P. Samanta, S. Mukherjee and S. K. Ghosh, *Chem.–Eur. J.*, 2015, **21**(3), 965–969; (*b*) K. M. Wang, L. Du, Y. L. Ma and Q. H. Zhao, *Inorg. Chem. Commun.*, 2016, **68**, 45–49; (*c*) Y. Deng, N. Chen, Q. Li, X. Wu, X. Huang, Z. Lin and Y. Zhao, *Cryst. Growth Des.*, 2017, **17**(6), 3170–3177; (*d*) W. Che, G. Li, X. Liu, K. Shao, D. Zhu, Z. Su and M. R. Bryce, *Chem. Commun.*, 2018, **54**, 1730–1733.
9 C. Behrend and K. Heesche-Wagner, *Appl. Environ. Microbiol.*, 1999, **65**(4), 1372–1377.
10 J. M. Sylvia, J. A. Janni, J. D. Klein and K. M. Spencer, *Anal. Chem.*, 2000, **72**(23), 5834–5840.
11 J. S. Caygill, F. Davis and S. P. Higson, *Talanta*, 2012, **88**, 14–29.
12 (*a*) S. Sandhu, R. Kumar, P. Singh, A. Mahajan, M. Kaur and S. Kumar, *ACS Appl. Mater. Interfaces*, 2015, **7**(19), 10491–10500; (*b*) K. Maiti, A. K. Mahapatra, A. Gangopadhyay, R. Maji, S. Mondal, S. S. Ali and D. Mandal, *ACS Omega*, 2017, **2**(4), 1583–1593; (*c*) B. Gogoi and N. Sen Sarma, *ACS Appl. Mater. Interfaces*, 2015, **7**(21), 11195–11202; (*d*) C. Wu, J. L. Zhao, X. K. Jiang, X. L. Ni, X. Zeng, C. Redshaw and T. Yamato, *Anal. Chim. Acta*, 2016, **936**, 216–221; (*e*) J. F. Xiong, J. X. Li, G. Z. Mo, J. P. Huo, J. Y. Liu, X. Y. Chen and Z. Y. Wang, *J. Org. Chem.*, 2014, **79**(23), 11619–11630.
13 (*a*) J. R. Zhang, Y. Y. Yue, H. Q. Luo and N. B. Li, *Analyst*, 2016, **141**(3), 1091–1097; (*b*) T. M. Geng, S. N. Ye, Y. Wang, H. Zhu, X. Wang and X. Liu, *Talanta*, 2017, **165**, 282–288.
14 (*a*) M. Kaur, S. K. Mehta and S. K. Kansal, *Sens. Actuators, B*, 2017, **245**, 938–945; (*b*) A. Pal, M. P. Sk and A. Chattopadhyay, *ACS Appl. Mater. Interfaces*, 2016, **8**(9), 5758–5762.
15 (*a*) A. Buragohain, M. Yousufuddin, M. Sarma and S. Biswas, *Cryst. Growth Des.*, 2016, **16**(2), 842–851; (*b*) H. Guo, Y. Zhang, Z. Zheng, H. Lin and Y. Zhang, *Talanta*, 2017, **170**, 146–151; (*c*) J. Ye, L. Zhao, R. F. Bogale, Y. Gao, X. Wang, X. Qian and G. Ning, *Chem.–Eur. J.*, 2015, **21**(5), 2029–2037; (*d*) S. Dang, J. H. Zhang and Z. M. Sun, *J. Mater. Chem.*, 2012, **22**(18), 8868–8873; (*e*) F. Y. Yi, J. P. Li, D. Wu and Z. M. Sun, *Chem.–Eur. J.*, 2015, **21**(32), 11475–11482; (*f*) W. T. Yang, H. R. Tian, J. P. Li, Y. F. Hui, X. He, J. Y. Li, S. Dong, Z. G. Xie and Z. M. Sun, *Chem.–Eur. J.*, 2016, **22**(43), 15451–15457.
16 G. M. Sheldrick, *SADABS, Program for Empirical Absorption Correction of Area Detector Data*, University of Göttingen, Göttingen, 1996.
17 P. van der Sluis and A. L. Spek, *Acta Crystallogr., Sect. A: Found. Crystallogr.*, 1990, **A46**, 194.
18 G. M. Sheldrick, *SHELXS 97, Program for Crystal Structure Refinement*, University of Göttingen, Göttingen, 1997.
19 J. Zhao, Y. N. Wang, W. W. Dong, Y. P. Wu, D. S. Li and Q. C. Zhang, *Inorg. Chem.*, 2016, **55**, 3265–3271.
20 (*a*) Y. L. Gai, F. L. Jiang, L. Chen, Y. Bu, K. Z. Su, S. A. Al-Thabaiti and M. C. Hong, *Inorg. Chem.*, 2013, **52**, 7658–7665; (*b*) A. D. Burrows, K. Cassar, T. Duren, R. M. W. Friend, M. F. Mahon, S. P. Rigby and T. L. Savarese, *Dalton Trans.*, 2008, **18**, 2465–2474; (*c*)

Open Access Article. Published on 13 June 2018. Downloaded on 5/2/2026 9:02:42 AM.
This article is licensed under a Creative Commons Attribution-NonCommercial 3.0 Unported Licence.

K. C. Xiong, F. L. Jiang, Y. L. Gai, Y. F. Zhou, D. Q. Yuan, K. Z. Su, X. Y. Wang and M. C. Hong, *Inorg. Chem.*, 2012, **51**, 3283–3288.

21 A. L. Spek, *J. Appl. Crystallogr.*, 2003, **36**, 7.

22 (*a*) J. Cao, Y. Gao, Y. Wang, C. Du and Z. Liu, *Chem. Commun.*, 2013, **49**(61), 6897–6899; (*b*) Y. L. Gai, F. L. Jiang, L. Chen, Y. Bu, K. Z. Su, S. A. Al-Thabaiti and M. C. Hong, *Inorg. Chem.*, 2013, **52**(13), 7658–7665.

23 (*a*) D. M. Chen, N. N. Zhang, C. S. Liu and M. Du, *J. Mater. Chem. C*, 2017, **5**(9), 2311–2317; (*b*) Y. Wang, H. Yang, G. Cheng, Y. Wu and S. Lin, *CrystEngComm*, 2017, **19**(48), 7270–7276; (*c*) X. Zheng, R. Fan, Y. Song, A. Wang, K. Xing, X. Du and Y. Yang, *J. Mater. Chem. C*, 2017, **5**(38), 9943–9951.

24 Y. Rachuri, B. Parmar, K. K. Bisht and E. Suresh, *Cryst. Growth Des.*, 2017, **17**(3), 1363–1372.

25 B. Chowdhury, S. Khatua, R. Dutta, S. Chakraborty and P. Ghosh, *Inorg. Chem.*, 2014, **53**(15), 8061–8070.

26 S. S. Nagarkar, A. V. Desai and S. K. Ghosh, *CrystEngComm*, 2016, **18**(17), 2994–3007.

27 (*a*) B. Q. Song, C. Qin, Y. T. Zhang, X. S. Wu, L. Yang, K. Z. Shao and Z. M. Su, *Dalton Trans.*, 2015, **44**(42), 18386–18394; (*b*) C. Zhang, Y. Yan, Q. Pan, L. Sun, H. He, Y. Liu and J. Li, *Dalton Trans.*, 2015, **44**(29), 13340–13346.

28 Y. Wang and Y. Ni, *Anal. Chem.*, 2014, **86**(15), 7463–7470.

29 (*a*) C. Hou, Y. Wang, Q. Ding, L. Jiang, M. Li, W. Zhu and M. Liu, *Nanoscale*, 2015, **7**(44), 18770–18779; (*b*) X. Lian and B. Yan, *Inorg. Chem.*, 2016, **55**(22), 11831–11838; (*c*) S. Wang, L. Shan, Y. Fan, J. Jia, J. Xu and L. Wang, *J. Solid State Chem.*, 2017, **245**, 132–137.

30 S. Mukherjee, A. V. Desai, A. I. Inamdar, B. Manna and S. K. Ghosh, *Cryst. Growth Des.*, 2015, **15**(7), 3493–3497.

This journal is © The Royal Society of Chemistry 2018